FACTA UNIVERSITATIS
Series: **Automatic Control and Robotics** Vol. 15, N^{o} 2, 2016, pp. 71 - 83

STUDY OF PERFORMANCE CHARACTERISTICS OF SINGLE PHASE MOTORS

UDC (621.313.33+(531.39+519.87)):621.3.012

Vasilija Sarac, Goce Stefanov, Goran Cogelja

University "Goce Delcev", Faculty of Electrical Engineering, Štip, Macedonia

Abstract. *Single phase shaded pole motor and permanently split capacitor motor are analyzed with double-filed revolving theory and method of symmetrical components is used for defining motor mathematical models. As an output from mathematical models steady-state performance characteristics of both motors are calculated for different operating regimes. Results from developed mathematical models are verified with experiments. Calculated currents of stator windings from mathematical models are used as input data in numerical models of the motors analyzed with Finite Element Method (FEM). Magnetic flux density in cross section of the motors is calculated from numerical motor models under different operating regimes. Parts of magnetic cores with high flux density are discovered and construction of the motors is further improved by applying soft magnetic powders.*

Key words: *single phase motors, performance characteristics, numerical models, finite element method*

1. INTRODUCTION

Single phase motors have wide application in many household devices since most small power (generally bellow 2 kW) induction machines have to operate with single phase a.c. power supplies that are readily available at homes and remote rural areas. As the name suggests, this type of motor has only one stator winding (main winding) while the rotor is a squirrel cage type. The single-phase induction motor is not a self-starting. When the motor is connected to single-phase supply the main winding carries, the altering current, which produces a pulsating magnetic filed. As the main magnetic filed is pulsating, torque necessary for the motor rotation is not generated. Consequently, it is necessary to have start/auxiliary winding. At single-phase shaded-pole motor (SPSPM) it is a short-circuit coil placed in stator poles while in permanently split capacitor motor (PSCM) it is a permanently connected capacitor in motor auxiliary winding. In this paper, two single-phase motors are

Received November 25, 2015
Corresponding author: Vasilija Sarac
Faculty of Electrical Engineering, Krste Misirkov, No.10-A, P.O 201 Štip, Macedonia
E-mail: vasilija.sarac@ugd.edu.mk

investigated: permanently split capacitor motor (PSCM), type FMR 35/6 and single-phase shaded pole motor (SPSPM) type AKO-16, both product of company MikronTech (Fig.1). Based on motor exact geometry, obtained from the producer, parameters of the motors are calculated. Method of symmetrical components based on double-field revolving theory is implemented as mathematical tool for calculation of motor performance characteristics [1-6]. Obtained values of characteristics from mathematical models are compared with data from experiment performed at producer premises. FEM models of motors are constructed, based on motor geometry, calculated parameters and characteristics of applied materials. Magnetic flux density distribution in cross-sections of the motors is obtained using time-harmonic approach, meaning all quantities are oscillating at frequency f=50 Hz and currents in rotor windings are freely induced.

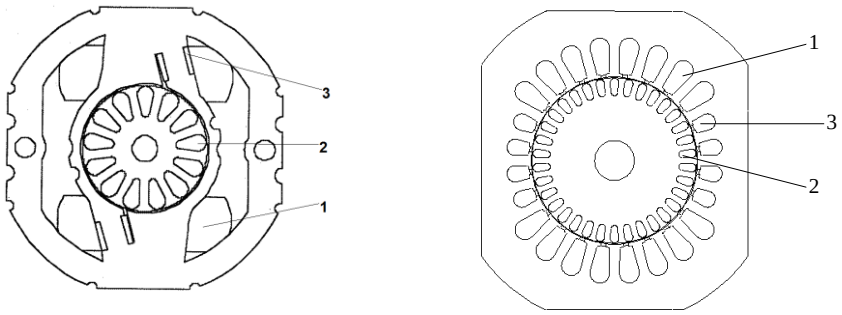

(a) SPSPM (b) PSCM

1-main stator winding, **2**-squirrel cage winding, **3**-auxiliary winding

Fig. 1 Cross section of single phase motors

2. PERFORMANCE CHARACTERISTICS

2.1 Mathematical models

During recent years, an extensive number of models of single-phase machines have been constructed in order steady-state and transient performance characteristics to be determined. Some authors propose motor model based on d-q transformation generally for calculation of transient characteristics of single-phase motors [7-9]. Others propose method of revolving filed polygon technique mainly applied for calculation of performance characteristics of single phase split-phase motors where the split phase (auxiliary) winding is replaced by a three phase winding which allows motor to be analyzed as symmetrical three phase motor under different operating regimes [10]. In this paper, calculation of performance characteristics of single-phase motors is based on double-field revolving theory and method of symmetrical components as a result of the existence of two stator windings mutually coupled one to another which produces elliptical electromagnetic field in machine air-gap. The unsymmetrical magnetomotive forces (mmf), currents and voltages corresponding to

the two windings of the single phase induction motor denoted as general vector **A** may be decomposed into two symmetrical systems (Fig. 2) consisted of forward and backward components (f&b) of the symmetrical systems [2]. On that way, all the electromagnetic processes inside the machine are analyzed as in the symmetrical three phase induction machine and all motor characteristics are obtained as sum of forward (direct "+") and backward (inverse "-") components.

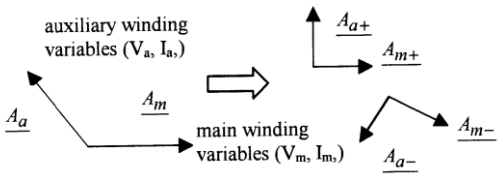

Fig. 2 Symmetrical components of two-phase system

From Fig. 2:

$$\underline{A_{a+}} = j\underline{A_{m+}} \;;\; \underline{A_{a-}} = -j\underline{A_{m-}} \tag{1}$$

The superposition principle yields:

$$\underline{A_m} = \underline{A_{m+}} + \underline{A_{m-}} \;;\; \underline{A_a} = \underline{A_{a+}} + \underline{A_{a-}} \tag{2}$$

Symmetrical components of variables associated to the main winding are found from:

$$A_{m+} = \frac{1}{2}(\underline{A_m} - j\underline{A_a}) \tag{3}$$

$$A_{m-} = \frac{1}{2}(\underline{A_m} + j\underline{A_a}) = \underline{A_{m+}^*} \tag{4}$$

The first step in calculation of performance characteristics is to determine all motor parameters: R_{sm}-main stator winding resistance, X_{sm}-main winding leakage reactance, R_{sa}-auxiliary stator winding resistance, X_{sa}-auxiliary stator winding leakage reactance, X_{mm}-the magnetizing reactance , R_{rm}-rotor winding resistance, X_{rm}-rotor winding leakage reactance, based on the motor dimensions and cross-section obtained from the producer (Fig.1). Afterwards direct and inverse impedances of main stator winding $\underline{Z_{m+}}$ and $\underline{Z_{m-}}$ are determined as well as mutual impedance between main and auxiliary winding $\underline{Z_a^m}$ and consequently they are used for calculation of direct and inverse components of current in main stator winding $\underline{I_{m+}}$ and $\underline{I_{m-}}$. Direct and inverse components of rotor winding impedance $\underline{Z_{r+}}$ and $\underline{Z_{r-}}$ are calculated as well [11]. They are used for calculation of direct and inverse components of rotor currents $\underline{I_{r+}}$ and $\underline{I_{r-}}$. Supply current is calculated from:

$$I_s = \left| \underline{I_{m+}} + \underline{I_{m-}} + j\frac{\underline{I_{m+}} - \underline{I_{m-}}}{a} \right| \tag{5}$$

Currents in main stator winding-I_m, auxiliary winding-I_a and rotor winding-I_r are calculated respectively:

$$I_m = \left|\underline{I_{m+}} + \underline{I_{m-}}\right| \qquad I_r = \left|I_{r+} + \underline{I_{r-}}\right| \tag{6}$$

$$I_a = \left| j\frac{\underline{I_{m+}} - \underline{I_{m-}}}{a} \right| \tag{7}$$

where *a* is the reduction ratio of auxiliary winding to main winding i.e. ratio between the number of turns of auxiliary stator winding-N_a and main winding-N_m. Developed electromagnetic power is calculated from parameters of rotor winding and motor slip-s:

$$P_{em} = \frac{2R_{rm}\left|I_{r+}\right|^2}{s} - \frac{2R_{rm}\left|I_{r-}\right|^2}{2-s} \tag{8}$$

Mechanical power is calculated from:

$$P_{mech} = P_{em}(1-s) \tag{9}$$

The motor output power is expressed as:

$$P_2 = \frac{P_{mech}}{1.015} \tag{10}$$

The motor output power is obtained from the mechanical power decreased by the value of stray losses, often difficult to be measured and IEEE-125 specifies them as 0.9-1.8% of the motor output power.

Direct and inverse components of motor torque are found from:

$$M_+ = \frac{2p}{\omega_1} I_{m+}^2 [\mathrm{Re}(\underline{Z_+}) - R_{sm}] \tag{11}$$

$$M_- = -\frac{2p}{\omega_1} I_{m-}^2 [\mathrm{Re}(\underline{Z_-}) - R_{sm}] \tag{12}$$

where p is the number of pair of poles and ω_1 is the angular frequency [rad/s]. Z_+ and Z_- are direct and inverse impedance obtained from main and rotor winding parameters as well as from magnetizing reactance [2].

Torque is obtained from:

$$M = M_+ + M_- \tag{13}$$

Input power is calculated from:

$$P_1 = V_s\left|I_s\right|\cos\varphi \tag{14}$$

V_s is the motor supply voltage, I_s is the supply current and $\cos\varphi$ is the power factor.

Power factor is calculated from:

$$\cos\varphi = \frac{real(I_s)}{I_s} \tag{15}$$

Efficiency factor is calculated from:

$$\eta = \frac{P_2}{P_1} \tag{16}$$

2.2. Results

Obtained values of motor characteristics calculated from mathematical modes are compared with data from experiment for the purpose of verification of proposed methodology and they are presented in Table 1 for PSCM at rated load operating point or motor slip-s of 0.04 and during motor start up or slip s=1. In Table 2 is presented comparison between measured and calculated data of SPSPM. Measurements of SPSPM are performed in faculty laboratory and further more they are compared with data from the producer.

Table 1 Comparison between calculated and measured data of PSCM

Rated operation, s=0.04		
Parameter	Mathematical model	Experiment
Rated torque M_n[Nm]	0.412	0.402
Rated supply current I_s [A]	1.6	1.32
Maximum output power P_2 [W]	215	210
Maximal torque M_{max} [Nm]	0.766	0.80
Start up , s=1		
Starting torque M [Nm]	0.1	0.13
Starting supply current I_s [A]	3.5	4

Presented results in Tables 2 and 3 have good similarity regarding obtained results from mathematical models in comparison with data from the experiments. This verifies the mathematical models of the motors as satisfactory accurate. In Fig.3 are presented performance characteristics of SPSPM with respect to the currents in all windings, efficiency factor η and power factor-cosφ for different motor slips. Characteristics of output torque-M_2 and electromagnetic torque-M_{em} of SPSPM are presented in Fig. 4.

Table 2 Comparison between calculated and measured data of SPSPM

Parameter	Mathematical model	Experiment	Producer
Rated current I_1 [A]	0.125	0.1259	0.18
Input power P_1[W]	18	18.114	22
Power factor cosφ [/]	0.6545	0.6538	0.555
Main st. wind. resistance R_{sm} [Ω]	498	493	480
No-load current I_0 [A]	0.111	0.1134	0.13
No load input power P_0 [W]	13.8	10.21	13.5
Short-circuit current I_k [A]	0.14	0.181	0.221
Short circuit power P_k [W]	19.87	29	31
Short-circuit p. f. cosφ_k [/]	0.6683	0.7389	0.6376

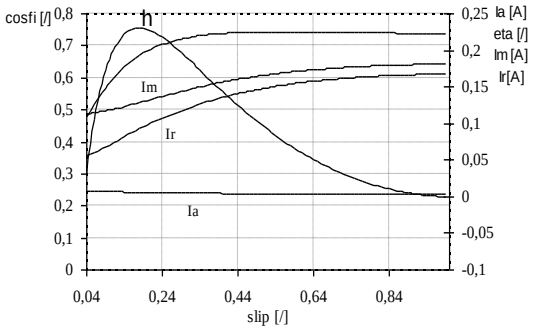

Fig. 3 Performance characteristics of currents, power factor and efficiency of SPSPM

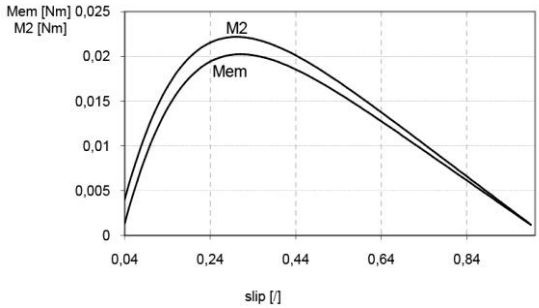

Fig. 4 Performance characteristics of torque of SPSPM

Characteristics of input and output power of SPSPM for different motor slips are presented in Fig. 5. In Figs. 6 and 7 are presented data from experiments performed on SPSPM. More specifically, in Fig.6 are presented characteristics of speed and input power of SPSPM for different voltages under rated load. In Fig 7 are presented results of main winding current and power factor for different voltages under rated load. In Fig.8 are presented characteristics of output torque-M_2, efficiency factor-η and power factor-cosφ obtained from mathematical model of PSCM.

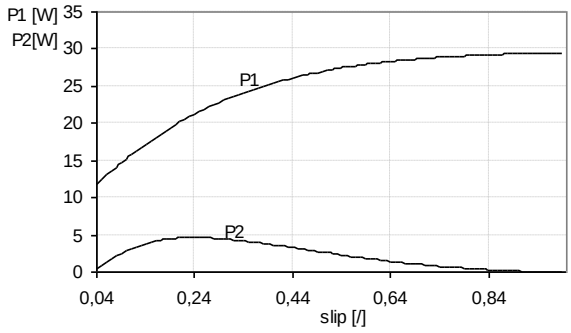

Fig. 5 Performance characteristics of input and output power of SPSPM

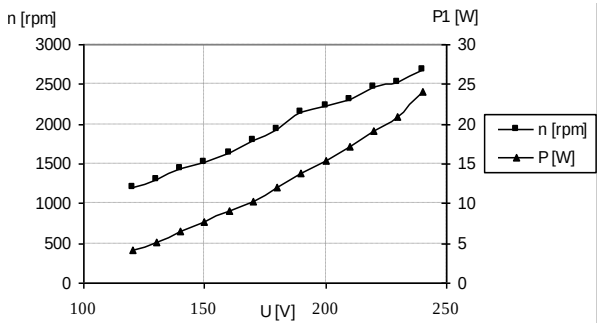

Fig. 6 Speed and input power of SPSPM from measurements

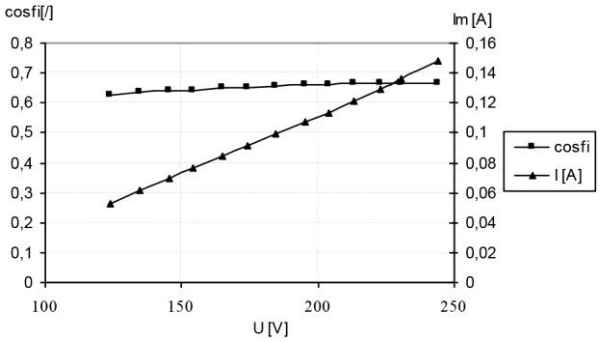

Fig. 7 Power factor and main winding current of SPSPM from measurements

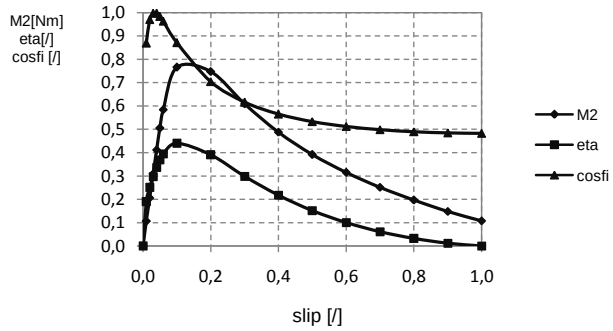

Fig. 8 Performance characteristics of output torque, power factor and efficiency of PSCM

Currents in all windings of PSCM: main, auxiliary and rotor are presented in Fig.9.

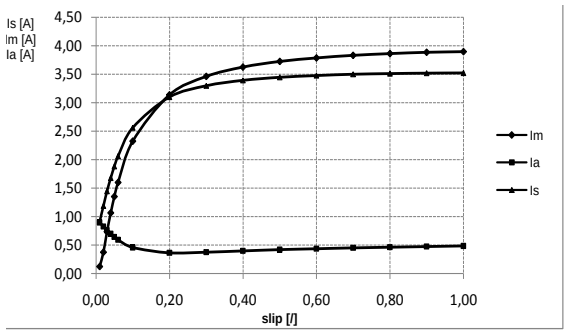

Fig. 9 Performance characteristics of currents of PSCM

In Fig.10 are presented characteristics of input and output power of PSCM.

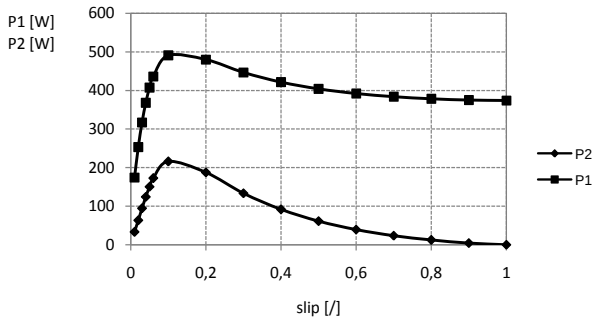

Fig. 10 Performance characteristics of input and output power of PSCM

3. FEM MODELS

Throughout the recent years, FEM has proved itself as valuable tool in electrical machine analysis when calculating parameters and characteristics of the variety of electromagnetic devices [12-15]. The analysis of the electromagnetic phenomena inside single-phase machines is always a challenging task due to the existence of the two stator windings mutually electromagnetically coupled, which together with the rotor winding produce an elliptic electromagnetic field in the motor air gap. Therefore, a special attention is paid on the proper motor modeling regarding current distribution in FEM model, by taking into account the currents in the main and the auxiliary stator winding and their phase displacement. Another important issue is the proper modeling of different operating regimes such as: no-load, rated load or locked rotor. Therefore, the rotor bars conductivity is adjusted to the motor slips correspondingly, i.e. the motor operating regime. Motors are analyzed for time-harmonic case, i.e. the currents are input only in the stator windings while in the rotor winding, the current is freely induced at frequency f=50 Hz due to the specific motor modeling. On that way, the analysis of electromagnetic phenomena inside the motor is closer to the real electromagnetic processes when the motor is supplied with voltage

220 V, 50 Hz. In order to determine the magnetic vector potential **A**, it is necessary the whole domain i.e. motor's cross-section to be divided into numerous elements (Figs. 11). When analyzing induction machines, considering their AC excitation, the air gap magnetic field is always a time-varying quantity. In the materials with non-zero conductivity, the eddy currents are induced, consequently the field problem turns into magneto-dynamic i.e. non-linear time-harmonic problem. When the rotor is moving, the rotor quantities oscillate at slip frequency. In this case, the rotor bars conductivity σ is adjusted correspondingly to the slip. Consequently, the following equation is going to be solved numerically:

$$\nabla x\left(\frac{1}{\mu(B)}\nabla x\mathbf{A}\right) = -\sigma\mathbf{A} + \mathbf{J_{src}} - \sigma\nabla V \tag{17}$$

where $\mathbf{J}_{src}$ represents the applied current sources [16]. The additional voltage gradient ΔV in 2-D field problems is constant over the conduction body.

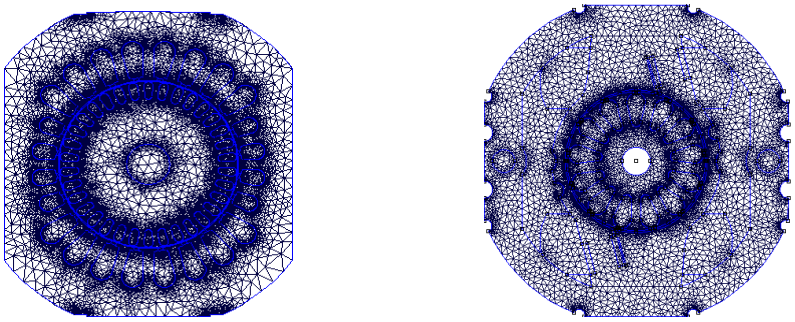

(a) PSCM (b) SPSPM

Fig. 11 Finite element mesh at cross-section of single phase motors

FEMM considers (17) for the case in which the field is oscillating at one fixed frequency. For this case, a phasor transformation yields a steady-state equation that is solved for the amplitude and phase of A. This transformation is:

$$A = \mathrm{Re}[a(\cos\omega t + j\sin\omega t)] = \mathrm{Re}[ae^{jwt}] \tag{18}$$

where a is the complex number. Substituting into (17) and dividing out the complex exponential term yields the equation that FEMM actually solves for harmonic magnetic problems:

$$\nabla x\left(\frac{1}{\mu_{ef}}\nabla xa\right) = -j\omega\sigma a + \mathbf{J_{src}} - \sigma\nabla V \tag{19}$$

in which $\mathbf{J}_{\mathbf{src}}$ represents the phasor transform of the applied current sources.

Strictly speaking, the permeability μ should be constant for harmonic problems. However, FEM retains a nonlinear relationship in the harmonic formulation, allowing the program

to approximate the effects of saturation on the phase and amplitude of the fundamental of the field distribution. The form of the BH curve is not exactly the same as in the DC case. Instead, "effective permeability" μ_{ef} is selected to give the correct amplitude of the fundamental component of the waveform under sinusoidal excitation. FEM also allows for the inclusion of complex and frequency-dependent permeability in time harmonic problems. These features allow the program to model materials with thin laminations and approximately model hysteresis effects [16].

In Figs. 12,13 and 14 is presented magnetic flux density distribution at cross-section of both motors for no-load, rated load and locked rotor, respectively.

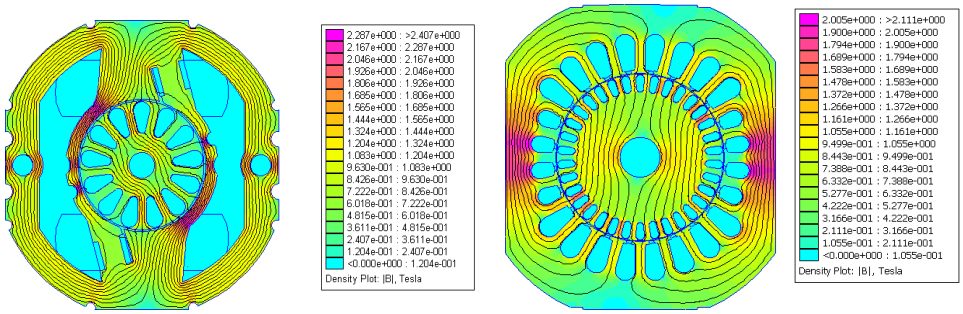

(a) SPSPM (b) PSCM

Fig. 12 Magnetic flux density distribution in motor cross-section-no load

From presented results in Figs. 12, 13 and 14 it is evident the presence of high values of magnetic flux density especially for SPSPM in the area of stator bridge which can be lowered by implementing high quality magnetic materials or soft magnetic powders at critical points of motor construction. In Fig. 16 is presented magnetic flux density distribution in cross-section of SPSPM for no-load, rated load and locked rotor operation with soft magnetic powder applied in construction of stator poles and bridge.

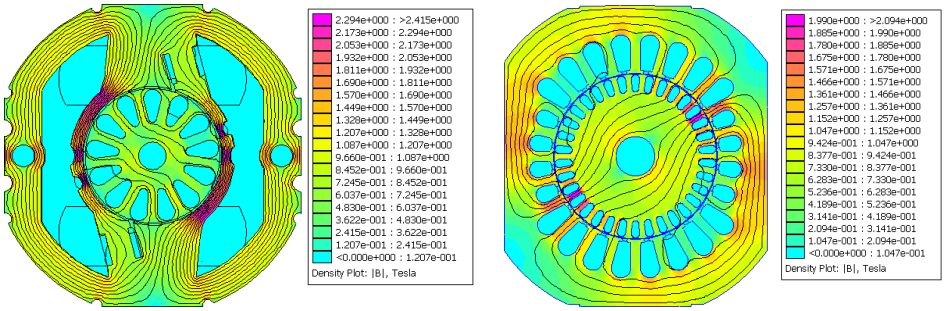

(a) SPSPM (b) PSCM

Fig. 13 Magnetic flux density distribution in motor cross-section-rated load

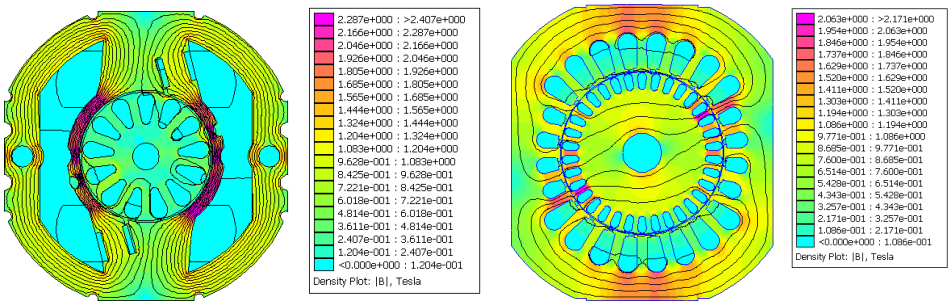

(a) SPSPM (b) PSCM

Fig. 14 Magnetic flux density distribution in motor cross-section-locked rotor

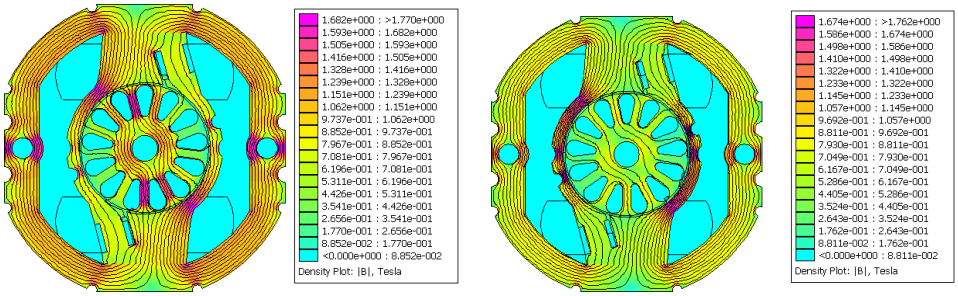

(a) no-load (b) rated load

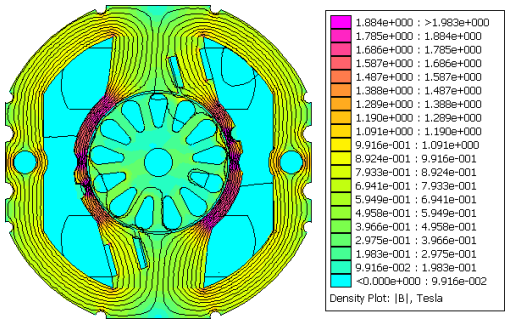

(c) locked rotor

Fig. 15 Magnetic flux density distribution-soft magnetic material in motor construction

From Fig.15 it is evident that application of soft magnetic material in construction of stator pole and bridge of SPSPM has contributed towards decrease of high values of magnetic flux density in stator bridge and consequently magnetic core saturation is avoided.

4. CONCLUSION

Two types of single-phase motors (shaded pole and permanently split capacitor) are analyzed under different operating regimes. Method of symmetrical components is applied as mathematical tool for obtaining parameters and characteristic of the motors. Proposed mathematical modes of the motors and obtained results from them are verified by experiments. Complete set of performance characteristics for different motor operating regimes i.e. different motor slips are plotted enabling motors operating regimes to be easily predicted and analyzed. Obtained parameters and characteristics are used as input data in FEM based motor models. FEM models are analyzed for time-harmonic case, when 220 V, 50 Hz is applied at motor power supply. As a result of FEM models magnetic flux density in motor cross- section is obtained. High value of magnetic flux density in stator bridge of shaded pole motor are observed. Therefore soft magnetic material is applied in construction of stator pole and bride of shaded pole motor resulting in lowered flux density in this critical part of the shaded pole motor. Obtained models enable accurate calculation of parameters and characteristics of analyzed motors, which improves overall motor design. Accuracy of developed numerical models of the motors is highly dependant on accurate calculation of parameters of the motors. Impedances of the motors are calculated with analytical formulas which give only approximate values of these parameters. Further authors' research will be focused on their numerical calculation which should improve overall accuracy of the design of these types of the motors.

REFERENCES

[1] W. H. Yeadon, A. W. Yeadon, *Handbook of small electric motors*. McGraww-Hill, New York, 2003.

[2] I. Boldea, S. A. Nasar, *The Induction Machines Design Handbook*. CRC Press, 2010.

[3] M. Popescu, T. J. Miller, M. McGilp, G. Strappazzon, N. Traivillin and R. Santarossa, "Asynchronous performance analysis of a single-phase capacitor-start, capacitor-run permanent magnet motor," IEEE Transactions on Energy Conversion, vol. 20, no. 1, pp. 142–150, 2005. [Online]. Available: http://dx.doi.org/10.1109/TEC.2004.837307

[4] G. Pessina, E. Morra, "Optimization and design of the shaded pole single phase asynchronous motor," in *International symposium power electronics, electrical drives, automation and motion*, SPEEDAM, Sorrento, Italy, pp. 469–473, 2012. [Online]. Available: http://dx.doi.org/10.1109/SPEEDAM.2012.6264407

[5] K. Makowski, M.J.Wilk, "Experimental verification of field-circuit model of a single-phase capacitor induction motor," Prezglad Electrotechniczny, vol. 88, no. 7b, pp. 116–118, 2012. [Online]. Available: http://pe.org.pl/articles/2012/7b/30.pdf

[6] S. H. Khader, "Modeling and simulation of single phase double capacitors induction motor," in *Proceedings of the 2nd WSEAS International Conference on biomedical electronics and biomedical informatics*, Moscow, Russia, pp. 21–27, 2009.

[7] K. Makowski, M. J. Wilk, "Determination of dynamic characteristics of the single phase capacitor induction motor," Prezglad Electrotechniczny, vol. 87, no.5, pp. 231–237, 2011. [Online]. Available: http://red.pe.org.pl/articles/2011/5/57.pdf

[8] S. Sunter, M. Odzemir, B. Gumus, "Modeling and simulation of single phase induction motor with adjustable switched capacitor," in *Proceedings of 9th International Conference on Power Electronics and Motion Control*, Kosice, Slovakia, pp.5–1–5–5, 2000.

[9] A. Leicht, K. Makowski, "Analysis of a single-phase capacitor induction motor operating at two power line frequencies," Archives of Electrical Engineering, vol. 61, no. 2, pp. 251–266, 2012. [Online]. Available: http://dx.doi.org/10.2478/v10171-012-0021-3

[10] C. B. Rasmussen, T. J. E.Miller, "Revolving-field polygon technique for performance prediction of single-phase induction motor," IEEE Transactions on Industry Applications, vol. 39, no. 5, pp. 1300–1306, 2003. [Online]. Available: http://dx.doi.org/10.1109/TIA.2003.816563

[11] I. E. Davidson, "Performance calculation of a shaded-pole single sided linear induction motor using symmetrical components and finite element method", Electromotion, vol. 4, no. 4, pp. 139–145, 1997.

[12] V. Hrabovcova, P. Rafajdus, "Radial magnetic forces of single phase permanent split-capacitor motor", Journal of Electrical Engineering, vol. 57, no. 4, pp. 185–192, 2006. [Online]. Available: http://iris.elf.stuba.sk/JEEEC/data/pdf/4_106-01.pdf

[13] A. Mladenović-Vučković, S. Aleksić, "Magnetic field determination for different block permanent magnet systems", Facta Universitatis, Series Electronics and Energetics, vol. 23, no. 3, pp. 259–272, 2010. [Online]. Available: http://dx.doi.org/10.2298/FUEE1003259V

[14] I. Popa, A-I. Dollan, "Numerical modeling of DC busbar contact", Facta Universitatis, Series Electronics and Energetics, vol. 24, no. 2., pp. 209–219, 2011. [Online]. Available: http://facta.junis.ni.ac.rs/eae/fu2k112as/5popa.pdf

[15] T. Vaimann, A. Belahcen, A.Kallaste, "Changing of magnetic-flux density distribution in a squirrel-cage induction motor with broken rotor bars", Elektronika ir Elektrotechnika, vol. 20, no. 7, pp. 11–14, 2014 [Online]. Available: http://dx.doi.org/10.1109/TEC.2004.837307

[16] D. Mekeer, "Finite element method magnetics-User's manual, version 4.2", 2010. [Online]. Available: http://www.femm.info/Archives/doc/manual42.pdf